Lumped and Distributed Device Embedding Techniques in Time Domain TLM Field Models

J.W. Park, P.P.M. So and W.J.R. Hoefer

Computational Electromagnetics Research Laboratory
Department of Electrical and Computer Engineering
University of Victoria
PO Box 3055, Victoria, BC, V8W 3P6, Canada

Email: JPark@ECE.UVic.CA

***Abstract* — There exist several techniques for embedding devices into TLM networks. These techniques yield in general slightly different results when the mesh size is finite. In this paper, we classify these techniques, compare results obtained with different embedding methods, and show how SPICE models of active and passive lumped element circuits can be incorporated into 2D and 3D TLM networks. Recommendations as to the best method for a given device type will be formulated.**

Keywords — Time Domain Modeling, TLM method, lumped device embedding, distributed device embedding, nonlinear devices, active devices, SPICE connection.

I. INTRODUCTION

TLM has the advantage that field equations are modeled in terms of transmission line networks, [1]. Embedding of lumped and distributed devices in the TLM mesh is thus rather straightforward since it involves only circuit connections. However, due to the discrete nature of TLM, the behavior of an embedded device will depend on its numerical implementation.

Lumped elements can be connected to a TLM mesh either at the nodes (center of the cells) or at the cell boundaries, [3] and [5], as shown in Fig. 1 for the 2D case. In many cases, the device may occupy a volume that exceeds the size of a single cell, yet the dimensions of this volume remain small compared to the wavelength. We are thus faced with a situation where the device is distributed over several TLM cells but remains quasi-lumped from a field perspective. The question thus arises how the device will interact with the field in such a situation. To show the effect of device connection and spreading over a number of nodes we have computed the S-parameters of a 50Ω resistor placed in a parallel plate waveguide. The width of the waveguide was discretized finely into 31 cells with a Δl =1mm. The resistor was connected to 1, 9, and 25 nodes in a manner shown in Figure 2, using both node and cell-boundary connections. In all cases, the volume occupied by the element remained small compared with the wavelength in the frequency range from 0 to 6 GHz.

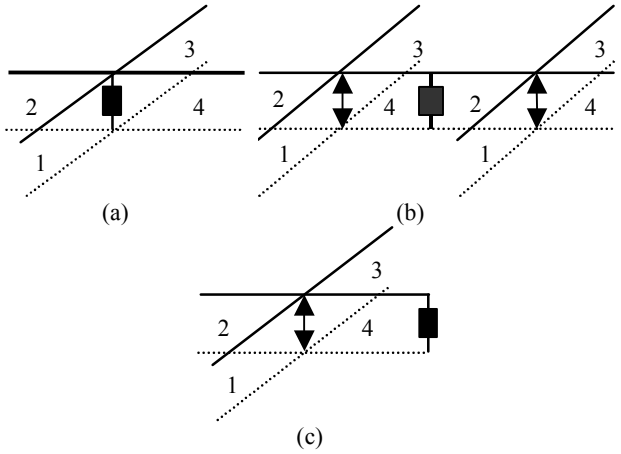

Fig. 1 Models for connecting lumped elements to a TLM network: (a) node connection, (b) cell boundary connection and (c) special case of cell boundary connection at the outer boundary of the computation domain. The TLM link lines are numbered 1 - 4.

Figure 3 compares the S-parameters obtained with the different embedding techniques. At very low frequencies, all device implementations converge to the theoretical value of |S11|=1/3 and |S21|=2/3. However, at higher frequencies, the effect of the finite size of the device due to its parasitic reactance becomes more pronounced, underlining the importance of spatial distribution of the equivalent elements. Node and boundary implementations also yield different responses even when the physical volume is the same in both cases. This is because the boundary model excludes the electromagnetic field completely from the volume it occupies.

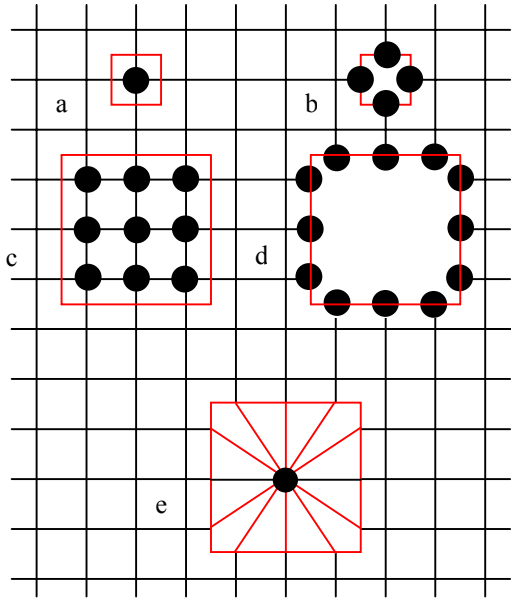

Fig. 2 Typical node and boundary implementations of lumped devices in a TLM mesh. (a) Single Node implementation (b) 1x1 boundary implementation (c) 3x3 node implementation (d) 3x3 boundary implementation (e) 3x3 star type implementation.

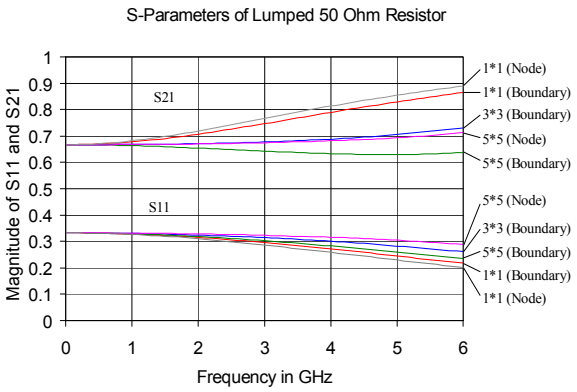

Fig. 3 S-Parameters of a lumped 50 Ohm resistor placed in a matched 50 Ohm parallel plate waveguide computed with TLM using different implementations outlined in Figure 2

The situation becomes more complex when nonlinear and, in particular, active nonlinear elements are to be embedded. From the physical point of view, it would be more realistic to spread the device over a finite volume corresponding to its physical size. However, if this results in the division of the equivalent circuit into several parallel devices, two types of problems arise.

1. Separate sub-devices are created which may interact in a parasitic fashion that is non-physical, involving the local properties of the discrete mesh. This may lead to instabilities due to the excitation of spurious oscillations.
2. The nonlinear differential equations must be solved separately for each sub-device, leading to increased computational demands.

In a three-dimensional situation, distributed devices that are spread over several cells in the direction of the applied voltage are implemented by connecting the nodes of the stacked cells in series and attaching one device to the stack. In the following, the implementation of active two-terminal devices using node and boundary implementations will be described.

II. Node Implementation of Active Devices

The first example described below is a push-pull oscillator comprising two identical Tunnel diodes. Figure 4 shows the oscillator featuring a slightly off-centered biasing arrangement. The nonlinear current-voltage characteristic of the diodes is specified in Table 1.

Table 1. Specifications of the Tunnel diodes used in the oscillator in Figure 4

Peak Current (I_p)	Peak Voltage (V_p)	Valley Current (I_v)	Valley Voltage (V_v)	Forward Peak Voltage (V_{fp})
1mA	65mV	0.14mA	350mV	510mV

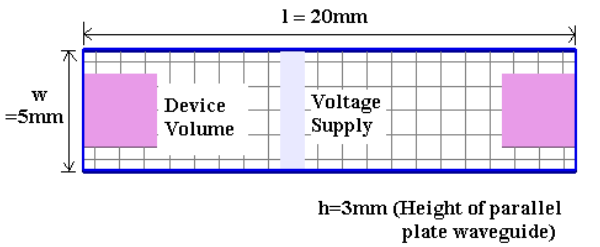

Fig. 4. The transmission line oscillator with biasing circuit.

In addition the diode had a series resistance of R_s=4.0Ω and a shunt capacitance of C_p=5pF. The I-V characteristic of the diode (Eq. 1) is plotted in Figure 5.

$$I = I_v \cdot \exp(V - V_v) + \frac{I_p \cdot V}{V_p} \exp(1 - \frac{V}{V_p}) + I_p \cdot \exp(\frac{V_{fp}}{V_{t1}}) \cdot \exp(\frac{V}{V_{t1}} - 1) \quad (1)$$

where V_{t1} = 26mV.

The biasing voltage is injected in a row of nodes slightly off-center of the push-pull circuit; it consists of an internal resistor and a DC voltage supply (V_s=200mV). The internal resistance must be determined such that the desired operating point (I_0,V_0) is established:

$$R_{\text{int}} = \frac{1}{2}\left(\frac{V_s - V_0}{I_0} - R_s \right) \qquad (2)$$

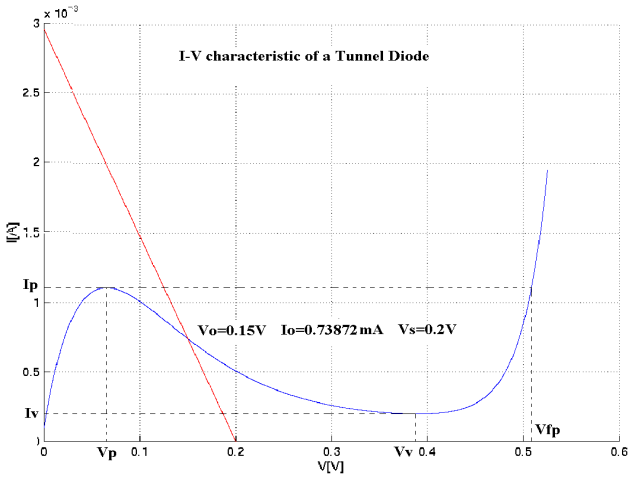

Fig. 5 I-V characteristic of a Tunnel diode.

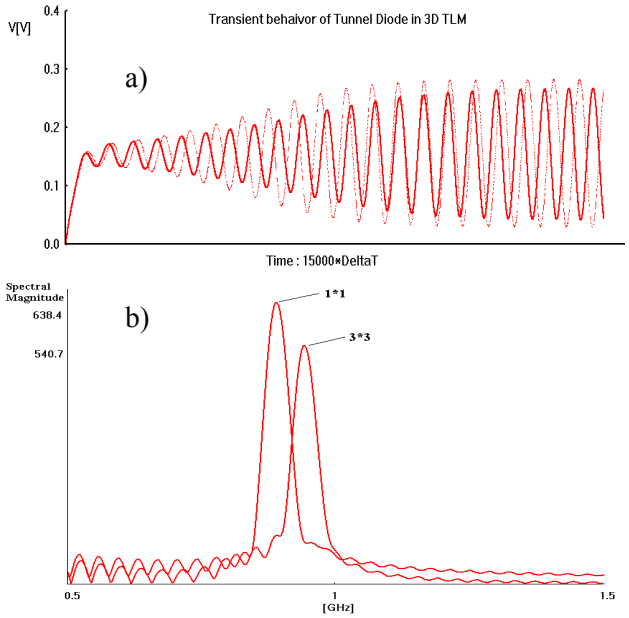

Fig. 6 Transient behavior (a) and frequency response (b) of the push-pull oscillator simulated by a 3D TLM network.

Figure 6 shows the transient behavior of the push-pull oscillator in which the diodes were embedded in a 3D TLM network using a $3\Delta l \times 3\Delta l \times 3\Delta l$ and a $1\Delta l \times 1\Delta l \times 1\Delta l$ node implementation, respectively. There is an obvious difference in the magnitude and phase of the two oscillators due to the differences in device volume and to the interaction between the separated sub-devices.

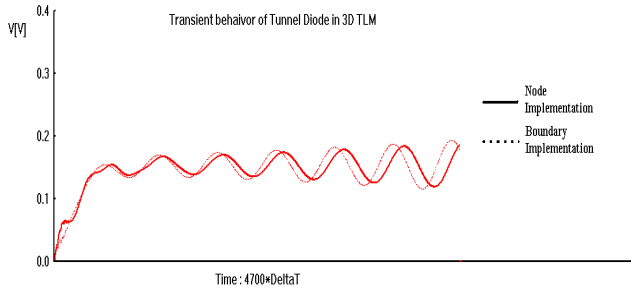

Fig. 7 Time domain responses of a Tunnel diode obtained with the node and boundary device embedding techniques.

Figure 7 depicts the time domain responses of the Tunnel diode oscillator when the diodes are occupying the same volume, but are implemented using node and boundary implementations. In the node implementations case, nine sub-devices are distributed over a $3\Delta l \times 3\ \Delta l \times 3\Delta l$ volume; in the boundary implementation case, twelve instead of 9 sub-devices are placed on the lateral surface of the diode volume, the outside part of the diode boundaries being open-circuited, as shown in Figure 4.

III. Star-Type Device Implementation

Figure 2(e) shows the star-type device implementation. It allows us to represent the device by a single lumped element that is connected centrally to N TLM transmission lines entering the boundary of the device volume. The star scattering matrix for this device-embedding scheme is:

$$\begin{bmatrix} {}_kV_s^r \\ {}_kV_1^r \\ {}_kV_2^r \\ {}_kV_3^r \\ \vdots \\ {}_kV_n^r \end{bmatrix} = \begin{bmatrix} 0 & 1/n & 1/n & 1/n & \cdots & 1/n \\ 1 & (1-n)/n & 1/n & 1/n & \cdots & 1/n \\ 1 & 1/n & (1-n)/n & 1/n & \cdots & 1/n \\ 1 & 1/n & 1/n & (1-n)/n & \cdots & 1/n \\ \vdots & \vdots & \vdots & \vdots & \cdots & \vdots \\ 1 & 1/n & 1/n & 1/n & \cdots & (1-n)/n \end{bmatrix} \cdot \begin{bmatrix} {}_kV_s^i \\ {}_kV_1^i \\ {}_kV_2^i \\ {}_kV_3^i \\ \vdots \\ {}_kV_n^i \end{bmatrix} \qquad (3)$$

Where ${}_kV_s^r$ represent the voltage impulses reflected on the star lines by the device at time step k, and ${}_kV_n^i$ are the incident voltage impulses on the n star lines. The voltage incident on the device is given by

$${}_kV_s^r = \frac{{}_kV_1^i + {}_kV_2^i + {}_kV_3^i + \cdots + {}_kV_n^i}{N} \qquad (4)$$

Note that the reference admittance for the device is chosen as N times the characteristic admittance of the star link lines. This condition decouples the incident and reflected voltage pulses of the device. Figure 8 shows the frequency response of the push-pull oscillator simulated by node implementation and star-line implementation in 2D-TLM, [2]. The frequency difference between these two implementations is a direct consequence of the differences in energy stored inside the device volume.

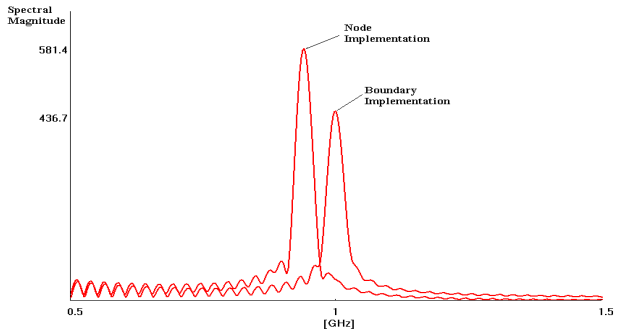

Fig. 8 Comparison of the frequency response of the push-pull diode oscillator simulated by the node and star-type device embedding techniques in 2D-TLM.

IV. The Connection between SPICE and TLM

TLM has the advantage that the electromagnetic field quantities are represented by voltages and currents in a network of transmission lines. This enables us to couple SPICE directly and easily [6][7] with TLM through a pipe. We can thus take full advantage of all existing device models in SPICE and do not need to formulate them again for TLM simulation. We can also perform noise analysis and account for temperature sensitivity of devices and other features supported by SPICE. However, the computational speed is somewhat reduced since SPICE must be called by TLM and run at each time step. Figure 9 shows a simple amplifier featuring an ideal BJT transistor inserted into a parallel-plate waveguide of size $3\,\Delta x \times 3\,\Delta y \times 20\,\Delta z$ where $\Delta x = \Delta y = \Delta z = \Delta l = 1$mm. The lumped resistive input and output voltage sources as well as the BJT transistor are inserted by means of stacked stubs. The source delivers V_s=0.88+0.08·sin(2πft) where f=220MHz, R_{int}=1200Ω, V_c=5V and R_c=377Ω. Figure 10 shows the collector-emitter voltage at the transistor obtained with a full SPICE simulation and with a coupled SPICE-TLM algorithm. Excellent agreement between the two results has been obtained. The extra capacitance introduced by the device stubs and the finite distance between the source and the transistor have been taken into account when creating the equivalent SPICE circuit.

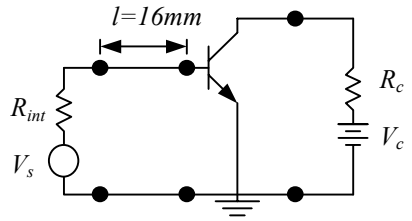

Fig. 9 A simple amplifier with BJT transistor.

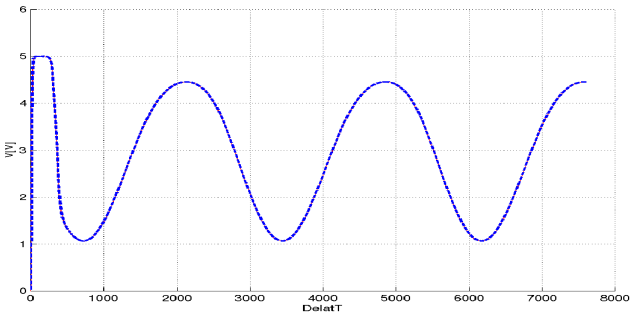

Fig. 10 The collector-emitter voltage computed with SPICE alone (dotted line) and with SPICE-TLM (solid line).

V. Conclusion

Properties of node, cell-boundary and star-type device embedding techniques for devices in 2D and 3D TLM networks have been investigated and compared. These techniques yield in general slightly different results when the mesh size is finite. A simple and powerful lumped element embedding approach has been developed by coupling SPICE with TLM.

References

[1] P. B. Johns, ***A symmetrical condensed node for the TLM method***, IEEE Trans. Microwave Theory Tech., vol. 35, pp. 370-377, Apr. 1987.

[2] P.P.M. So, Eswarappa and W.J.R. Hoefer, ***A Two-dimensional Transmission Line Matrix Microwave Field Simulator Using New Concepts and Procedures***, IEEE MTT, vol. 37, no 12, pp. 1877-1884, December 1989.

[3] P. Russer, P. P. M. So, and W. J. R. Hoefer, ***Modeling of nonlinear active regions in TLM***, IEEE Microwave Guided Wave Letter, vol. 1, pp. 10-13, Jan. 1991.

[4] P. Russer, M. Righi, C. Eswarappa, and W. Hoefer, ***Lumped element equivalent circuit parameter extraction of distributed microwave circuits via TLM simulation***, in IEEE MTT-S Digest, pp. 887-890, 1994.

[5] L. Cascio, G. Tardioli, and W. Hoefer, ***Modeling of nonlinear active and passive devices in three dimensional TLM networks***, in IEEE MTT-S Digest, pp. 383-386, 1997.

[6] P. Antognetti, G. Massobrio, ***Semiconductor Device Modeling with SPICE***, McGraw-Hill, New York, 1987.

[7] W. Banzhaf, ***Computer-Aided Circuit Analysis Using SPICE***, Prentice Hall, New Jersey, 1989.